ChemComm

COMMUNICATION

Control over the synthesis of homovalent and mixed-valence cubic cobalt-imidazolate cages†

Liang Liang,‡[b] Dong Luo,‡[a] Tao Zuo,[a] Xiao-Ping Zhou *[a] and Dan Li *[a]

Cite this: *Chem. Commun.*, 2019, **55**, 5103

Received 14th March 2019,
Accepted 1st April 2019

DOI: 10.1039/c9cc02083g

rsc.li/chemcomm

A series of cubic cobalt-imidazolate cages have been successfully synthesized *via* subcomponent self-assembly in different solvents under solvothermal conditions. The homovalent Co^{II} and mixed-valence $Co^{III,II}$-imidazolate cages are assembled with control over the mixed solvent ratio of *N*,*N*-diethylformamide/ethanol, respectively.

Metal–organic cages (MOCs) with unique confined cavities have been widely studied in recent years due to their exquisite structures and advanced functions[1] (*e.g.*, recognition and sensing,[2–4] stabilization of reactive species,[5–7] and catalysis[8–10]). A giant number of MOCs with varied geometries including tetrahedron,[6,11] cube,[12,13] octahedron,[9,14] rhombic dodecahedron,[15,16] and dodecahedron[17] *etc.* have been obtained by elaborately prepared ligands and selected metal ions. Usually, the metal ions are homovalent. However, some metal ions (*e.g.* cobalt and iron ions) are easily oxidized or reduced. Controlling the valence of metal ions is important, because of the probable influences on the MOCs' properties.

Solvothermal synthesis has been developed as a useful approach to construct metal–organic framework (MOF) and MOC materials. Some unprecedented structures can be obtained by using solvothermal synthesis, in which *in situ* generation of organic ligands and oxidation/reduction of metal ions are easily performed.[18–22] On the other hand, scientists have found that structures of MOCs can be obtained by varying some subtle factors (*e.g.* ligand bend angle,[23] template,[24] and solvent[25]). However, the control of the valence of metal ions in MOCs is almost undeveloped,[26–29] especially for solvothermal synthesis.

The sub-component self-assembly technology developed by Nitschke *et al.*[30] is a convenient and feasible method for the assembly of MOCs. In our previous study, we successfully obtained a series of polynuclear metal-imidazolate cages (metal = Ni, Co, and Zn) by sub-component self-assembly.[13,16,28,29] In the present work, we describe the control over assembly of a family of cubic eight-nucleus homovalent and mixed-valent Co-imidazolate cages. The homovalent Co-imidazolate cage is neutral, formulated as $[Co_8^{II}L_{12}Br_4]\cdot x$solvents (**1a**, L = HL1 = *N*-((5-methyl-1*H*-imidazol-4-yl)methylene)(4-bromophenyl)methanamine; **2**, L = HL2 = *N*-((5-methyl-1*H*-imidazol-4-yl)methylene)(4-fluorophenyl)methanamine). The mixed-valence Co-imidazolate cage has a charge of 4+, formulated as $[(Co^{III}{}_4Co^{II}{}_4L_{12}Br_4)\cdot 3Br\cdot NO_3]\cdot x$solvents (**1b**, L = HL1; **3**, L = HL3 = *N*-((5-methyl-1*H*-imidazol-4-yl)methylene)(4-methylphenyl)-methanamine; **4**, L = HL4 = *N*-((5-methyl-1*H*-imidazol-4-yl)-methylene)(4-trifluoromethylphenyl)methanamine) (Scheme 1). The cages have been characterized and investigated *via* single crystal X-ray diffractions, powder X-ray diffraction (PXRD), elemental analyses, Fourier transform infrared (FT-IR), mass spectrometry, UV-Vis-NIR, cyclic voltammetry, and magnetic susceptibility. Interestingly, the valences of the Co ions in the cages can be tuned by varying the ratio of mixed solvents, providing a good example of controlling the metal valence of MOCs.

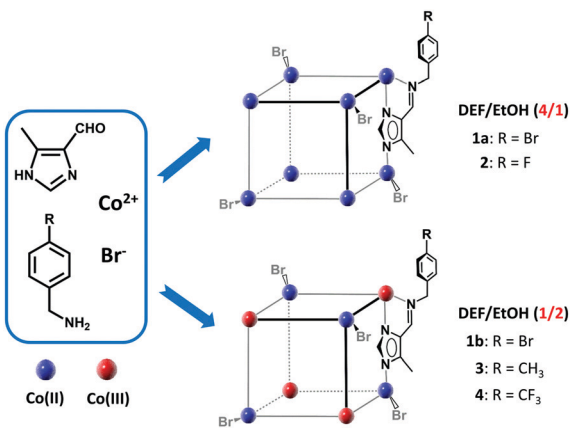

Scheme 1 Illustration of subcomponent self-assembly of homovalent and mixed-valence cubic Co-imidazolate cages under different reaction conditions.

[a] *College of Chemistry and Materials Science, Jinan University, Guangzhou, Guangdong 510632, P. R. China. E-mail: zhouxp@jnu.edu.cn, danli@jnu.edu.cn*
[b] *Department of Chemistry, Shantou University, Shantou, Guangdong 515063, P. R. China*

† Electronic supplementary information (ESI) available: Experimental section, characterization and physical measurements. CCDC 1872745–1872749. For the ESI and crystallographic data in CIF or other electronic format see DOI: 10.1039/c9cc02083g

‡ These authors contributed equally to this work.

One-pot multicomponent reactions of 5-methyl-imidazole-4-carboxaldehyde, $Co(NO_3)_2{\cdot}6H_2O$, NaBr and different 4-R-benzylamines (R = bromo, fluoro, methyl, and trifluoromethyl) in mixed solvents of *N*,*N*-diethylformamide (DEF)/ethanol (EtOH) with different volume ratios at 120 °C under solvothermal conditions yielded appreciable single crystals of **1a**, **1b**, **2** and **3**, and a powder of **4**, respectively (Scheme 1; see the ESI† for details). **4** shows good solubility in *N*,*N*-dimethylformamide (DMF). Single crystals of **4** were then obtained by slow diffusion of diethyl ether into its DMF solution. PXRD and elemental analysis data of these cages showed that the bulk samples were of a pure phase (see the Experimental section of the ESI† and Fig. S4–S8).

Single crystals of **1a**, **1b**, **2**, **3** and **4** were measured by X-ray diffraction (XRD) analyses. These cages crystallize in the $P\bar{4}3n$ (**1a**, **2**), $C2/c$ (**1b**, **3**) and $Fddd$ (**4**) space groups, respectively (see Tables S1 and S2 for detailed crystallographic data in the ESI†). They all feature eight-nucleus cubic Co_8L_{12} structures with tetrahedral and octahedral metal centres as vertices and imidazolate ligands as edges (Fig. 1 and Fig. S1, ESI†). As examples, the crystal structures of **1a** and **1b** will be described in detail.

As shown in Fig. 1a and b, four Co ions with octahedral coordination geometry adopt an alternating arrangement model at the cube metal nodes relative to the other four metal centres with tetrahedral coordination geometry in cages **1a** and **1b**. L1 serves as a bridge to connect two types of metal nodes. L1 was *in situ* generated, which is further documented by using FT-IR spectra with obvious C=N specific absorbance bands at 1606 cm^{-1} (see Fig. S2, ESI†). The structural differences between **1a** and **1b** are reflected in the following two aspects: (1) difference of Co–N coordination bond lengths; (2) difference in the nature of the cavity. In the octahedral Co centre, the Co–N bond length is 2.091(9) Å for **1a**, while that of **1b** ranges from 1.883(6) to 1.916(6) Å. The obviously shorter Co–N bonds of **1b** indicate that the octahedral Co centres of **1b** have +3 oxidation state[28,29,31] and those of **1a** feature +2 oxidation state. For the tetrahedral Co centres, the Co–N bond length of **1a** is 1.973(9) Å, which is similar to that of **1b** (1.982(7) to 2.006(8) Å). Thus, the tetrahedral Co centres for both cages are in +2 oxidation state. As shown in Fig. 1a and b, there is no guest anion in the cavity of **1a**, but a Br^- anion is encapsulated in the cavity of **1b**. Based on the above analysis, we propose that cage **1a** probably shows electric neutrality with homovalent Co^{II} ions, while cage **1b** has electric positive properties with mixed-valence $Co^{II/III}$ ions.

Cages **1a** and **1b** were synthesized under similar solvothermal reaction conditions except for the different volume ratios (DEF/EtOH of 4/1 for **1a** and 1/2 for **1b**, respectively) of the mixed solvents used. To further test the influence of the solvent ratio on the results, different substituents of 4-R-benzylamines (R = fluoro, methyl, and trifluoromethyl) were selected as reaction components. Homovalent cage **2** was obtained in the DEF/EtOH ratio of 4/1, while mixed-valence cages **3** and **4** were formed from that of 1/2. Under solvothermal conditions, it is expected that the oxidation of Co^{II} may happen in the reaction process due to the presence of a small amount of oxygen in the reaction system. The fact that a homovalent Co^{II} cage was generated from a higher DEF content implies that the oxidation of Co^{II} may be inhibited under such a condition. The reducibility of

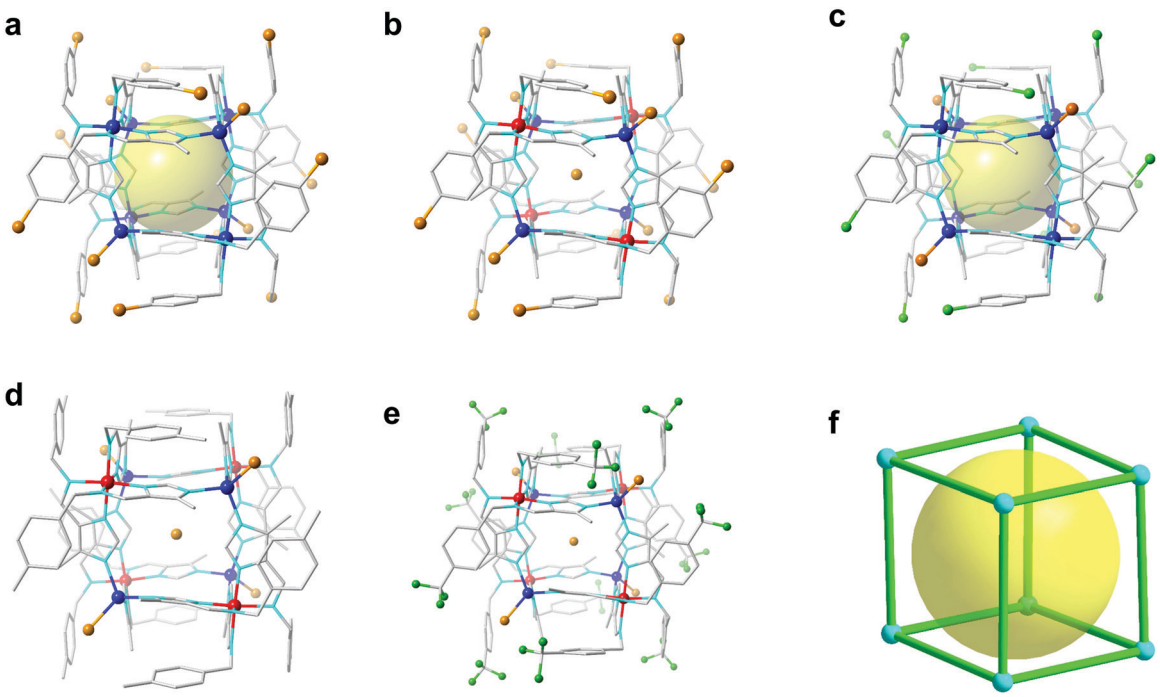

Fig. 1 Single-crystal structures of cubic Co-imidazolate cages **1a** (a), **1b** (b), **2** (c), **3** (d) and **4** (e). Simplified topology of these cubic cages (f). The big yellow ball represents the cavity in the cages without the Br^- guest. Color codes for elements: Co^{II} blue, Co^{III} red, N cyan, C gray, F green, and Br orange. Hydrogen atoms are omitted for clarity.

DEF under solvothermal conditions is likely to stop the oxidation of Co^{II} to Co^{III}. When the proportion of DEF is low in the mixed solvent, Co^{II} tends to be oxidized to Co^{III} by oxygen. The strategy of adjusting the ratio of mixed solvents provides a means of controlling the synthesis of homovalent and mixed-valence Co-imidazolate cages, which is rarely observed in MOC preparations.[28,29]

1b is slightly soluble in the methanol and acetonitrile mixture (1/1, v/v) after ultrasonic treatment, **3** has limited solubility in methanol and **4** shows very good solubility in methanol. The atmospheric pressure ionization or electrospray ionization-time of flight (API or ESI-TOF) mass spectra of cage **1b** (Fig. 2 and Fig. S10, ESI†), cage **3** (Fig. S11, ESI†) and cage **4** (Fig. S12, ESI†) were recorded to identify the stability of the cages in solution. The prominent peaks of cage **1b** correspond to formula $\{[Co_8(L1)_{12}Br_4]\cdot x Br\cdot y NO_3\}^{(4-n)+}$ (x = 0–2, y = 0–2, n = 1–2) and the experimental isotope distributions are in good agreement with the simulated patterns (inset in Fig. 2 and Fig. S10, ESI†). Mass spectra manifest that Co-imidazolate cages **1b**, **3**, and **4** are successfully prepared and remain stable without decomposition in solution.

The UV-Vis-NIR absorption spectrum (380–1000 nm) of mixed-valence **1b** gives three obvious absorption bands at 478 nm, 614 nm and 910 nm (Fig. S13, ESI†). The first absorption band at 478 nm can be attributed to the electronic transitions from the $^1A_{1g}$ ground state to the $^1T_{1g}$ excited state of the octahedral coordination geometry Co^{III} ions in the chromophore $[Co^{III}Im_3N_3]$.[32] The other two absorption bands in the visible region at 614 nm and in the near-IR region at 910 nm correspond to the electronic transitions from the $^4A_2(F)$ ground states to the excited states $^4T_1(F)$ and $^4T_1(P)$ of the tetrahedral coordination geometry Co^{II} ions in the chromophore $[Co^{II}Im_3Br]$.[33] The absorption spectrum of homovalent **1a** shows no significant difference compared with that of mixed-valence **1b** in absorption positions. However, the absorption peak intensities of **1a** and **1b** are different at the same concentrations. This distinction should be attributed to the Co valence difference in these two cages, which affected the electronic transition probability of different coordination configuration chromophores and resulted in different absorbance of the UV-Vis-NIR absorption spectra.

In order to investigate the redox properties of **1a** and **1b** in solution, cyclic voltammetry (CV) was utilized for monitoring the electrochemical behaviour. For the CV curve of **1b**, there are two irreversible reduction peaks at −1.17 V and −2.01 V, which could be assigned to $Co^{III/II}$ and $Co^{II/I}$ couples of reduction processes, respectively (Fig. S14, ESI†). The further scan exhibits enhanced current at potential near the $Co^{II/I}$ couple and the currents increased markedly at more negative potential which was assigned to the reduction process of Co^I to Co^0.[34] An irreversible oxidation peak at 0.93 V was assigned to the $Co^{II/III}$ couple of the oxidation process. Compared with **1b**, the CV of cage **1a** showed two irreversible reduction peaks at −1.04 V and −2.17 V and an oxidation peak at 1.22 V (Fig. S14, ESI†). The presence of low $Co^{III/II}$ and $Co^{II/I}$ reduction states in the cage is important in terms of its possible utility in applications of electrochemical and (electro)catalytic reactions (*e.g.* reduction of CO_2).

To further confirm the oxidation state of Co centres in **1a** and **1b**, magnetic properties were studied. The temperature dependence of magnetic susceptibility of crystalline samples **1a** and **1b** was measured at a range of 2–300 K in a field of 2000 Oe (Fig. S15 and S16, ESI†). The $\chi_M T$ *versus* T curves of **1a** and **1b** showed the typical character of antiferromagnetic exchange between Co centres below about 20 K (Fig. 3a and b). For the single d^7 Co^{II} ion, when it is in a high-spin state (S = 3/2) the $\chi_M T$ spin-only value is 1.87 cm^3 K mol^{-1}; when it is in a low-spin state (S = 1/2) the $\chi_M T$ spin-only value is 0.37 cm^3 K mol^{-1} (room temperature, see the ESI† for details). From Fig. 3a, the observed maximum $\chi_M T$ value of cage **1a** at about 300 K is 9.77 cm^3 K mol^{-1}, which is close to the spin-only value of 8.96 cm^3 K mol^{-1}. This result reveals that four Co^{II} ions are in

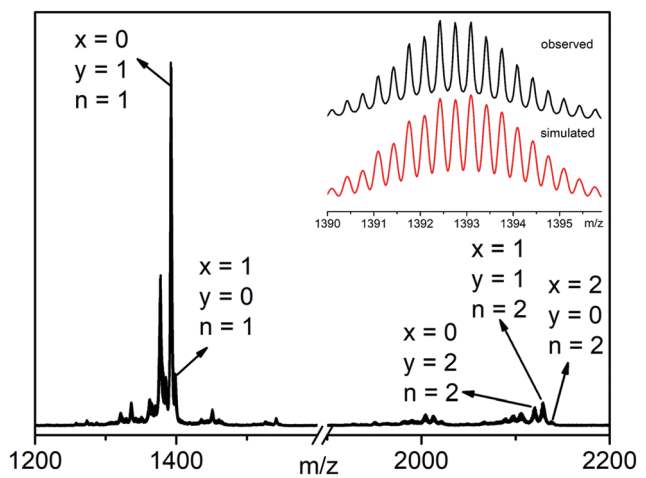

Fig. 2 API-TOF mass spectrum of cage **1b**. The prominent peaks correspond to formula $\{[Co_8(L1)_{12}Br_4]\cdot x Br\cdot y NO_3\}^{(4-n)+}$, x = 0–2, y = 0–2, n = 1–2. The inset shows the observed and simulated isotopic patterns of the peaks at an m/z ratio of 1392.43 corresponding to the species of $\{[Co_8(L1)_{12}Br_4]\cdot NO_3\}^{3+}$.

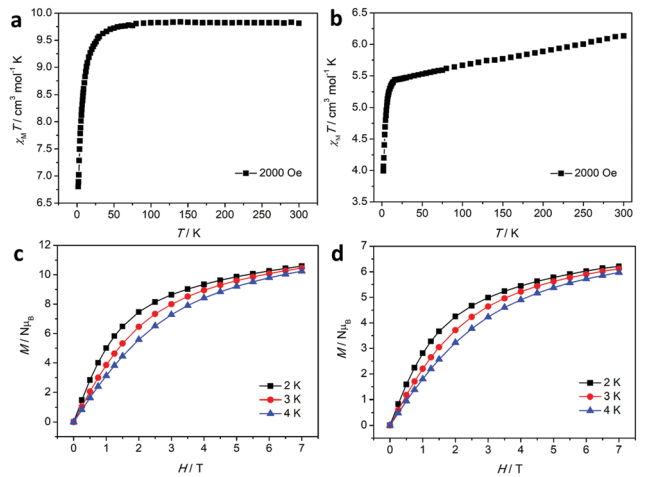

Fig. 3 Temperature dependence of the $\chi_M T$ (plots of $\chi_M T$ *versus* T) for (a) **1a** and (b) **1b** measured in the 2000 Oe field and the field dependence of magnetization (plots of M *versus* H) for (c) **1a** and (d) **1b** at 2 K (black), 3 K (red), and 4 K (blue), respectively.

high-spin state and the other four Co^{II} ions are in low-spin state. This $\chi_M T$ value of **1a** agrees with no orbital contribution to the magnetic effective moment, which is probably due to completely quenched orbital momentum of the octahedral coordination low-spin (^2E_g ground state contains three unpaired electrons in the t_2 orbitals) and tetrahedral coordination high-spin ($^4A_2$ ground state has one unpaired electron in an e_g orbital) d^7 Co^{II} centres. For cage **1b** (Fig. 3b), the maximum $\chi_M T$ value is 6.24 cm^3 K mol^{-1}, which is slightly lower than the spin-only value of 7.48 cm^3 K mol^{-1} with four high-spin ($S = 3/2$) d^7 Co^{II} ions at about 300 K. This is probably due to the lack of strong antiferromagnetic coupling between the Co centres. The low $\chi_M T$ value of **1b** agrees with its mixed valence property. The octahedral coordination d^6 Co^{III} ions are probably in a diamagnetic low-spin state with no unpaired electrons ($S = 0$), while the tetrahedral coordination d^7 Co^{II} ions probably adopt a high-spin state with three unpaired electrons.

In addition, the field dependence isothermal magnetization of **1a** and **1b** was measured at 2 K, 3 K and 4 K, respectively (Fig. 3c and d). The magnetization of **1a** and **1b** at 2 K is increased slowly with the increase of the magnetic field. The field dependent magnetization at the highest field of 8 T is 10.4 Nβ for **1a** and 6.6 Nβ for **1b**, which corresponds to below the saturation value of 16 Nβ (per Co_8 cage unit with spin-only included four high-spin and four low-spin d^7 Co^{II} ions) and 12 Nβ (per Co_8 cage unit with spin-only included four high-spin d^7 Co^{II} ions and four low-spin d^6 Co^{III} ions). These data further suggest the presence of antiferromagnetic interactions in **1a** and **1b**. Moreover, the measurement of AC susceptibility was performed for **1a** and **1b** in the AC field of 0 and 1000 Oe (Fig. S17–S24, ESI†). The in-phase (χ') and out-of-phase (χ'') components exhibit no obvious peaks in the range of 2–20 K and no frequency dependent oscillation at 100 and 997 Hz. These results indicate that there was no long-range order in crystalline cages **1a** and **1b**.

Taken together, we successfully constructed a series of homovalent and mixed-valence cubic Co-imidazolate cages by solvothermal subcomponent self-assembly. The oxidation state of Co ions in the cages can be effectively regulated by controlling the proportion of the DEF/EtOH mixed solvent. Magnetic measurements further confirm the valence state of cages **1a** and **1b** and show the antiferromagnetic exchange between Co centres in the Co-imidazolate cages. These homovalent and mixed-valence cubic Co-imidazolate cages provide successful examples for valence controllability by rational regulation of reacting solvents for synthesizing MOCs. Furthermore, studies on the application of electrocatalytic and photocatalytic chemical reactions by using homovalent and mixed-valence Co-imidazolate cages are ongoing.

We thank Professor Yan-Zhen Zheng (Xi'an Jiaotong University) for measuring magnetic susceptibility. This work was financially supported by the National Natural Science Foundation of China (No. 21731002, 91222202, 21871172 and 21371113), the Guangdong Natural Science Funds for Distinguished Young Scholars (2014A030306042), and the Training Program for Excellent Young College Teacher of Guangdong Province and Jinan University.

Conflicts of interest

There are no conflicts to declare.

Notes and references

1 T. R. Cook and P. J. Stang, *Chem. Rev.*, 2015, **115**, 7001–7045.
2 C.-L. Liu, R.-L. Zhang, C.-S. Lin, L.-P. Zhou, L.-X. Cai, J.-T. Kong, S.-Q. Yang, K.-L. Han and Q.-F. Sun, *J. Am. Chem. Soc.*, 2017, **139**, 12474–12479.
3 D. Zhang, T. K. Ronson, J. Mosquera, A. Martinez, L. Guy and J. R. Nitschke, *J. Am. Chem. Soc.*, 2017, **139**, 6574–6577.
4 W. Xuan, M. Zhang, Y. Liu, Z. Chen and Y. Cui, *J. Am. Chem. Soc.*, 2012, **134**, 6904–6907.
5 M. Yamashina, Y. Sei, M. Akita and M. Yoshizawa, *Nat. Commun.*, 2014, **5**, 4662.
6 P. Mal, B. Breiner, K. Rissanen and J. R. Nitschke, *Science*, 2009, **324**, 1697–1699.
7 K. Li, L.-Y. Zhang, C. Yan, S.-C. Wei, M. Pan, L. Zhang and C.-Y. Su, *J. Am. Chem. Soc.*, 2014, **136**, 4456–4459.
8 D. M. Kaphan, M. D. Levin, R. G. Bergman, K. N. Raymond and F. D. Toste, *Science*, 2015, **350**, 1235–1238.
9 C. Tan, J. Jiao, Z. Li, Y. Liu, X. Han and Y. Cui, *Angew. Chem., Int. Ed.*, 2018, **57**, 2085–2090.
10 X. Jing, C. He, Y. Yang and C. Y. Duan, *J. Am. Chem. Soc.*, 2015, **137**, 3967–3974.
11 F. J. Rizzuto, D. M. Wood, T. K. Ronson and J. R. Nitschke, *J. Am. Chem. Soc.*, 2017, **139**, 11008–11011.
12 M. D. Ward, C. A. Hunter and N. H. Williams, *Chem. Lett.*, 2017, **46**, 2–9.
13 D. Luo, M. Li, X. P. Zhou and D. Li, *Chem. – Eur. J.*, 2018, **24**, 7108–7113.
14 D. O. M. Fujita, M. Miyazawa, H. Oka, K. Yamaguchi and K. Ogura, *Nature*, 1995, **378**, 469–471.
15 Z. Lu, C. B. Knobler, H. Furukawa, B. Wang, G. N. Liu and O. M. Yaghi, *J. Am. Chem. Soc.*, 2009, **131**, 12532–12533.
16 X. P. Zhou, J. Liu, S. Z. Zhan, J. R. Yang, D. Li, K. M. Ng, R. W. Y. Sun and C. M. Che, *J. Am. Chem. Soc.*, 2012, **134**, 8042–8045.
17 B. Olenyuk, M. D. Levin, J. A. Whiteford, J. E. Shield and P. J. Stang, *J. Am. Chem. Soc.*, 1999, **121**, 10434–10435.
18 X. M. Chen and M. L. Tong, *Acc. Chem. Res.*, 2007, **40**, 162–170.
19 P. Cui, H. S. Hu, B. Zhao, J. T. Miller, P. Cheng and J. Li, *Nat. Commun.*, 2015, **6**, 6331.
20 H. C. Hu, H. S. Hu, B. Zhao, P. Cui, P. Cheng and J. Li, *Angew. Chem., Int. Ed.*, 2015, **54**, 11681–11685.
21 D. Li, T. Wu, X. P. Zhou, R. Zhou and X. C. Hitang, *Angew. Chem., Int. Ed.*, 2005, **44**, 4175–4178.
22 P. R. Symmers, M. J. Burke, D. P. August, P. I. T. Thomson, G. S. Nichol, M. R. Warren, C. J. Campbell and P. J. Lusby, *Chem. Sci.*, 2015, **6**, 756–760.
23 Q. F. Sun, J. Iwasa, D. Ogawa, Y. Ishido, S. Sato, T. Ozeki, Y. Sei, K. Yamaguchi and M. Fujita, *Science*, 2010, **328**, 1144–1147.
24 I. A. Riddell, M. M. J. Smulders, J. K. Clegg, Y. R. Hristova, B. Breiner, J. D. Thoburn and J. R. Nitschke, *Nat. Chem.*, 2012, **4**, 751–756.
25 B. Kilbas, S. Mirtschin, R. Scopelliti and K. Severin, *Chem. Sci.*, 2012, **3**, 701–704.
26 J. M. Breen, R. Clerac, L. Zhang, S. M. Cloonan, E. Kennedy, M. Feeney, T. McCabe, D. C. Williams and W. Schmitt, *Dalton Trans.*, 2012, **41**, 2918–2926.
27 S. J. Ferrara, B. Wang and J. P. Donahue, *Dalton Trans.*, 2016, **45**, 2997–3002.
28 D. Luo, X. P. Zhou and D. Li, *Angew. Chem., Int. Ed.*, 2015, **54**, 6190–6195.
29 D. Luo, X. Z. Wang, C. Yang, X. P. Zhou and D. Li, *J. Am. Chem. Soc.*, 2018, **140**, 118–121.
30 J. R. Nitschke, *Acc. Chem. Res.*, 2007, **40**, 103–112.
31 M. H. Alkordi, J. L. Belof, E. Rivera, L. Wojtas and M. Eddaoudi, *Chem. Sci.*, 2011, **2**, 1695–1705.
32 E. H. Clifford, J. Hawkins, J. Martin, J. A. L. Palmer and M. R. Snow, *Aust. J. Chem.*, 1986, **39**, 1213–1220.
33 A. Klanicova, Z. Travnicek, I. Popa, M. Cajan and K. Dolezal, *Polyhedron*, 2006, **25**, 1421–1432.
34 E. A. Fluegel, V. W. h. Lau, H. Schlomberg, R. Glaum and B. V. Lotsch, *Chem. – Eur. J.*, 2016, **22**, 3676–3680.

